IOP Publishing Journal of Geophysics and Engineering
J. Geophys. Eng. **12** (2015) 26–32 doi:10.1088/1742-2132/12/1/26

Seismic attenuation in fractured media

Ying Rao[1,2] **and Yanghua Wang**[2]

[1] State Key Laboratory of Petroleum Resources and Prospecting, China University of Petroleum (Beijing), People's Republic of China
[2] Centre for Reservoir Geophysics, Department of Earth Science and Engineering, Imperial College London, UK

E-mail: raoying@cup.edu.cn and yanghua.wang@imperial.ac.uk.

Received 5 August 2014, revised 20 October 2014
Accepted for publication 27 October 2014
Published 9 December 2014



Abstract

The prime objective of this paper is to quantitatively estimate seismic attenuation caused by fractures with different physical parameters. In seismic wave simulation, the fractured media are treated as the anisotropic media and fractures are represented by frequency-dependent elastic constants. Based on numerical experiments with three different parameters, namely viscosity, porosity and the Lamé parameters, this paper has the following observations. First, seismic attenuation is not affected by the viscosity within fractures, although it increases with the increase of porosity and decreases with the increase of the Lamé parameters within fractures. Among the latter two parameters, seismic attenuation is more sensitive to the Lamé parameters than to the porosity. Second, for the attenuation anisotropy, low frequencies have more anisotropic effect than high frequencies. For example, a 50 Hz wavefield has the strongest anisotropy effect if compared to 100 and 150 Hz wavefields. The attenuation anisotropy for low frequency (say 50 Hz) is more sensitive to the viscosity than the porosity and the Lamé parameters have the weakest effect among these three parameters. These observations suggest that low-frequency seismic attenuation, and especially the attenuation anisotropy in low frequency, would have great potential for fluid discrimination within fractured media.

Keywords: attenuation, attenuation anisotropy, fracture, numerical solutions, computational seismology

1. Introduction

Fractures are a critically important element in reservoir characterisation and for its efficient development. Hudson *et al* (1996) and Chapman (2003) developed theoretical models of attenuation caused by sparse concentration of saturated penny-shaped fractures. Shen and Toksöz (2000) studied scattering characteristics in fractured reservoirs using the coherent part of reflected seismic waves and pointed out that attenuation can be determined from the scattering characteristics in fractured reservoirs. Based on seismic attenuation, Rao and Wang (2009) reconstructed fracture distribution using waveform tomography.

In fractured reservoirs, the fluid-filled fractures cause frequency-dependent wave attenuation, which could show significant effects on observed seismic wavefields (Thomsen 1995, Hudson *et al* 2001, Tod 2001, Maultzsch *et al* 2003). Based on Biot's theory of poroelasticity (Biot 1962), Brajanovski *et al* (2005) pointed out that saturated fractures cause significant attenuation due to wave-induced fluid flow between fractures. In addition, the elastic properties of fractured media are dependent upon the isolated fluid-filled fractures in a solid background at high frequencies. But at low frequencies, the elastic properties of fractured media satisfy the anisotropic Gassmann (or Brown–Korringa) theory applied to a porous material with linear-slip interfaces. Vlastos *et al* (2007) showed that scattering attenuation is not only frequency dependent but also related to the direction of propagation and the orientation of the fractures. That is the attenuation anisotropy.

Most of the previous work focused on the effect of the geometric property of fractures. The prime objective of this paper is to quantitatively evaluate wave attenuation caused by fractures defined with different physical parameters, such as viscosity, porosity and the Lamé parameters, within the fractures. Frequency-dependent seismic response of fractures is simulated by wave equation modelling in the equivalent anisotropic media, in which fractures are incorporated into finite-differencing grids using an effective medium theory (Coates

 © 2015 Sinopec Geophysical Research Institute Printed in the UK

Downloaded from https://academic.oup.com/jge/article/12/1/26/5110308 by Imperial College London Library user on 17 August 2020

and Schoenberg 1995, Liu *et al* 2000, Hudson *et al* 2001). This theory can deal with fracture scattering without having any limitation on the number of fractures within the media

We attempt to investigate fractures that have characteristics of continuous, parallel-walled layers, filled with weak solid (Liu *et al* 2000, Hall and Wang 2012). These fractures can be a good representation of common hydraulic fractures, allowing fluids (water, oil or gas) to flow more readily to the wellbore (Liu and Martinez 2013). Physically, the elastic constants that represent these fractures are frequency dependent. Therefore, a frequency-domain wave equation method is used in this paper to investigate seismic wave propagations in general anisotropic media which take account of fractures.

This paper numerically evaluates the effects of viscosity, porosity and Lamé parameters within fractures and plane wave frequencies on the horizontal attenuation, the vertical attenuation and the attenuation anisotropy by analysing the scattered wavefield that propagates through a cluster of fractures. The investigation reveals that low-frequency attenuation and especially the attenuation anisotropy at low frequencies, would have a great potential for fluid discrimination within fractured media.

2. Seismic response of fractures

Frequency-domain wave equations in (2D) space are defined as (Hall and Wang 2009, Wang 2011)

$$
\begin{aligned}
-\omega^2\rho u = {} & \frac{\partial}{\partial x}\left(c_{11}\frac{\partial u}{\partial x}\right)+\frac{\partial}{\partial z}\left(c_{51}\frac{\partial u}{\partial x}\right)+\frac{\partial}{\partial x}\left(c_{15}\frac{\partial u}{\partial z}\right)\\
& +\frac{\partial}{\partial z}\left(c_{55}\frac{\partial u}{\partial z}\right)+\frac{\partial}{\partial x}\left(c_{13}\frac{\partial v}{\partial z}\right)+\frac{\partial}{\partial x}\left(c_{15}\frac{\partial v}{\partial x}\right)\\
& +\frac{\partial}{\partial z}\left(c_{53}\frac{\partial v}{\partial z}\right)+\frac{\partial}{\partial z}\left(c_{55}\frac{\partial v}{\partial x}\right)\ ,\\
-\omega^2\rho v = {} & \frac{\partial}{\partial x}\left(c_{51}\frac{\partial u}{\partial x}\right)+\frac{\partial}{\partial x}\left(c_{55}\frac{\partial u}{\partial z}\right)+\frac{\partial}{\partial z}\left(c_{31}\frac{\partial u}{\partial x}\right)\\
& +\frac{\partial}{\partial z}\left(c_{35}\frac{\partial u}{\partial z}\right)+\frac{\partial}{\partial x}\left(c_{53}\frac{\partial v}{\partial z}\right)+\frac{\partial}{\partial x}\left(c_{55}\frac{\partial v}{\partial x}\right)\\
& +\frac{\partial}{\partial z}\left(c_{33}\frac{\partial v}{\partial z}\right)+\frac{\partial}{\partial z}\left(c_{35}\frac{\partial v}{\partial x}\right)\ ,
\end{aligned}
\tag{1}
$$

where u and v are the horizontal and vertical displacements, ω is the angular frequency, ρ is the bulk density and c_{ij} are the elastic constants of the stiffness tensor in Hook's law.

For a 2D model, discretising equation (1) with a second-order finite-differencing scheme yields a matrix-vector equation as

$$\mathbf{Mu} = \mathbf{s}, \tag{2}$$

where $\mathbf{M}$ is a complex-valued matrix approximating partial differential operators, $\mathbf{u}$ is a vector representing the two displacement components over all node points and $\mathbf{s}$ is a vector representing a source term (zero everywhere except at the grid of the source). In order to improve the accuracy, a 45° rotated coordinate frame is combined to the original second-order finite-differencing star. This coupling produces an equivalent accuracy of a fourth-order finite-differencing scheme (Štekl and Pratt 1998).

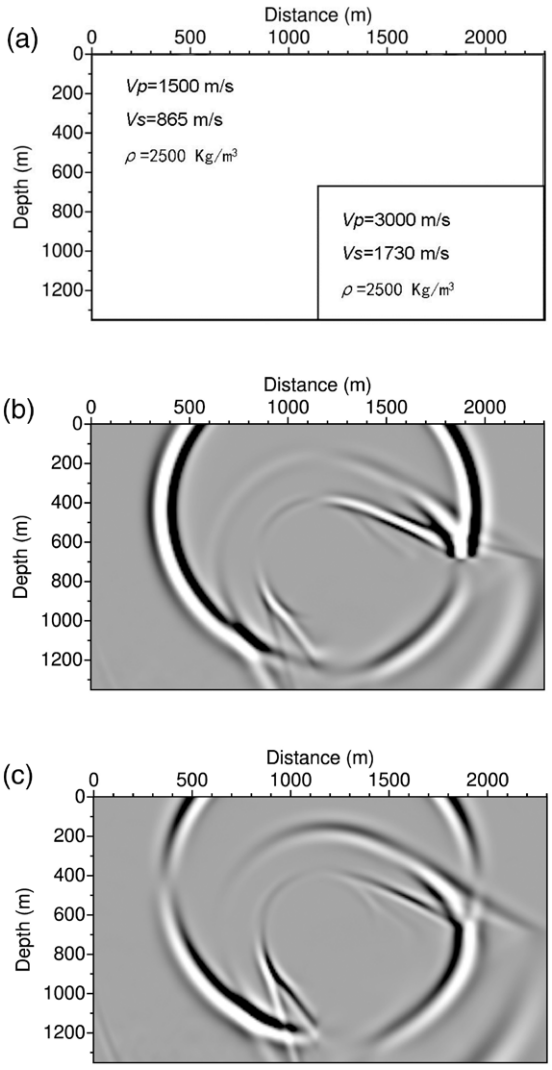


Figure 1. (*a*) The geometry of a corner-edge model. (*b, c*) Snapshot of horizontal and vertical components of wave propagation after time 625 ms.

Figure 1(*a*) is a corner-edge model designed for testing the quality of a finite difference scheme (Hall and Wang 2009). The *P*-wave velocity of the upper medium is 1500 m s^{-1} and S-wave velocity is 865 m s^{-1}, while the lower corner medium has a *P*-wave velocity of 3000 m s^{-1} and *S*-wave velocity of 1730 m s^{-1}. The density of the medium is $\rho = 2500\,\mathrm{kg\,m^{-3}}$. In a homogeneous, isotropic media, $c_{11} = c_{33} = \lambda + 2\mu$, $c_{13} = c_{31} = \lambda$ and $c_{55} = \mu$, where λ and μ are Lamé parameters and $c_{15} = c_{51} = c_{35} = c_{53} = 0$. A *P*-wave point source is used for this wave simulation. Figures 1(*b*) and (*c*) show snapshots of horizontal and vertical components respectively, which show clear features of reflections, refractions and diffractions. When the wavefront reaches the corner, part of the energy is transmitted into the corner block and part is reflected back from both sides of the corner. The diffracted energy from the corner can also be observed. For the four artificial model boundaries, as a 45 degree absorbing boundary condition is used, there are no significant boundary reflections. This example demonstrates the effectiveness of the frequency-domain wave equation method.

Downloaded from https://academic.oup.com/jge/article/12/1/26/5110308 by Imperial College London Library user on 17 August 2020

One of the advantages of the frequency-domain modelling method is the convenience of taking account of any frequency-dependent effect such as attenuation in waveform modelling by simply replacing real-valued variables with complex-valued variables in the wave equation (Rao and Wang, 2009, Wang and Rao 2009).

For modelling fractured media, a fracture is expressed as a boundary with discontinuous displacement and continuous stress and fractured media are represented as anisotropic media by using the equivalent media theory (Schoenberg 1980, Coates and Schoenberg 1995, Liu *et al* 2000). Then the elastic constants c_{ij} are given as the following (Schoenberg 1980),

$$\begin{aligned} c_{11} &= (\lambda+2\mu)\left(1+\frac{\lambda+2\mu}{\mu}\phi C_N\right)^{-1}, \\ c_{33} &= [\,(\lambda+2\mu)+4\,(\lambda+\mu)\,\phi C_N]\left(1+\frac{\lambda+2\mu}{\mu}\phi C_N\right)^{-1}, \\ c_{13} &= c_{31} = \lambda\left(1+\frac{\lambda+2\mu}{\mu}\phi C_N\right)^{-1}, \\ c_{55} &= \mu(1+\phi C_T)^{-1}. \end{aligned} \tag{3}$$

Physical meanings of all involved parameters are given as the following:

(1) λ and μ , the Lamé parameters of background materials. Note that if ϕ is set to zero, constants c_{ij} represent locally the isotropic, homogeneous medium.

(2) ϕ, the porosity of the fractured material which is defined as (Liu *et al* 2000)

$$\varphi = \frac{N_f S d}{V}, \tag{4}$$

where d is the average fracture aperture, N_f is the number of fractures within the fractured region, V is the volume of the fractured region and S is the mean area of fractures.

(3) C_N and C_T, dimensionless parameters defined by the shear module μ normalised by Lamé parameters and viscosity inside the fracture, as (Schoenberg 1980, Liu *et al* 2000)

$$\begin{aligned} C_N &= \frac{\mu}{\lambda_f+2\mu_f+i\frac{4}{3}\omega\eta_f}, \\ C_T &= \frac{\mu}{\mu_f+i\omega\eta_f}, \end{aligned} \tag{5}$$

where λ_f and μ_f are the Lamé parameters of the infill materials including fluid and η_f is their viscosity.

Analysing equation (5), we have the following observations:

(a) As C_N and C_T for representing fractures are frequency dependent, all elastic constants c_{ij} in equation (2) are frequency dependent. Thus, we implement wave simulation in the frequency domain. The elastic constants are also complex valued, because of complex values C_N and C_T.

(b) For a given η_f, its actual effect depends upon the frequency. Generally speaking, the latter acts as a scalar working on the viscosity.

(c) When we rewrite equation (5) as $C_N = |\,C_N\,|\exp(i\theta_N)$ and $C_T = |\,C_T\,|\exp(i\theta_T)$, we have the amplitudes as

$$\begin{aligned} |C_N| &= \frac{\mu}{\sqrt{\left(\lambda_f+2\mu_f\right)^2+\left(\frac{4}{3}\omega\eta_f\right)^2}}, \\ |C_T| &= \frac{\mu}{\sqrt{\mu_f^2+(\omega\eta_f)^2}}. \end{aligned} \tag{6}$$

These quantities indicate that viscosity η_f of the infill materials does not have much effect, compared to the potential effect of the Lamé parameters λ_f and μ_f. This is because, in the two denominators, the magnitude of λ_f and μ_f is about $10^5 - 10^6$ order and the magnitude of η_f is about $10^{-1} - 10^0$ order, and in the seismic band the frequency has the magnitude order of $10^0\pi - 10^2\pi$

(d) Equation (6) also suggests that the effect of the Lamé parameters can be seen more clearly in low frequencies, where $(\omega\eta_f)^2$ is small in comparison to $\left(\lambda_f+2\mu_f\right)^2$ or μ_f^2.

(e) We also have the phase terms defined as

$$\begin{aligned} \theta_N &= -\tan^{-1}\left(\frac{\frac{4}{3}\omega\eta_f}{\lambda_f+2\mu_f}\right), \\ \theta_T &= -\tan^{-1}\left(\frac{i\omega\eta_f}{\mu_f}\right). \end{aligned} \tag{7}$$

These quantities suggest that viscosity η_f will cause linear phase delay (negative valued) for plane waves with various frequencies. According to the definition of seismic quality factor, Q, this phase delay (i.e. the ratio of the imaginary part to the real part) is a measurement of seismic attenuation, Q^{-1} (Wang 2008).

This current study is on wet fractures. So compared to Vlastos *et al* (2007), Rao and Wang (2009) and Hall and Wang (2012), the crack density is replaced with porosity within the fracture and two constants representing a compact cluster of dry cracks are replaced with C_N and C_T, to represent fluid-filled fractures.

Note that the definition above assumes that fractures are parallel to the direction of c_{11}. Therefore, a rotation matrix should be applied to model fractures with different orientations. As pointed out by Hall and Wang (2012), the Love notation of the elastic constant as second order c_{ij}, although a convenient form, is not a true second order tensor and cannot be rotated as such in the finite difference grid. It is necessary to return to the original full fourth-order tensor $c_{ijk\ell}$, before applying rotation.

3. Seismic attenuation caused by fractures

Equations (3) and (5) indicate that, in general, porosity ϕ, viscosity η_f and the Lamé parameters $\lambda_f + 2\mu_f$ of fracture infill materials have direct effects on the wavefield. We are going to evaluate the attenuation effect with respect to these parameters.

For the following tests, we build a model of $800 \times 800\,\mathrm{m}^2$ in size (figure 2(*a*)). The background solid matrix (without fractures) has P-wave velocity $V_P = 4000\,\mathrm{m\,s^{-1}}$, S-wave velocity V_S

Downloaded from https://academic.oup.com/jge/article/12/1/26/5110308 by Imperial College London Library user on 17 August 2020

$= 2000\,\mathrm{m\,s^{-1}}$ and density $\rho = 2500\,\mathrm{kg\,m^{-3}}$. The corresponding Lamé parameters are $\lambda = 2\times10^7\,\mathrm{KPa}$ and $\mu = 10^7\,\mathrm{KPa}$.

For fractures, the porosity is set to be 10%, the viscosity η_f is 0.5 KPa·s and the Lamé parameters $\lambda_f + 2\mu_f = 10^6\,\mathrm{KPa}$. The horizontal and vertical components of a plane wavefield for a *P*-wave source propagation with frequency of 150 Hz are displayed in figures 2(*b*) and (*c*), respectively.

When considering attenuation, Q^{-1}, the plane wavefield may be expressed as (Wang 2004)

$$A(r) = A_0 \exp\left(-\frac{\omega r}{2c_R Q}\right), \tag{8}$$

where $A(r)$ is the amplitude at distance r, A_0 is the initial amplitude at reference point $r = 0$, and c_R is the real-valued velocity. Equation (8) indicates that, although Q is frequency independent, the attenuation is frequency dependent. Note that A_0 is also the amplitude at distance r without any attenuation, $Q^{-1} = 0$. That is, $A(r)\big|_{Q^{-1}=0} = A_0$. Diffraction of fractures causes wave attenuation. Therefore, the attenuation can be extracted by

$$Q^{-1}(r) = -\frac{c_R}{\omega r}\ln\left(\frac{A^2(r)\big|_{Q^{-1}\neq 0}}{A_0^2}\right). \tag{9}$$

In the following experiments, this attenuation measurement of the horizontal component wavefield is defined as Q_x^{-1}, and that of the vertical component wavefield is defined as Q_z^{-1}.

Once $Q_x^{-1}(r)$ and $Q_z^{-1}(r)$ are estimated, the attenuation anisotropy can be evaluated as

$$\gamma \equiv \frac{Q_x^{-1}(r)}{Q_z^{-1}(r)} = \frac{\ln\left[A_0^2\right] - \ln\left[A^2(r)\big|_x\right]}{\ln\left[A_0^2\right] - \ln\left[A^2(r)\big|_z\right]}. \tag{10}$$

If the background wavefield is normalised to the unity, $\ln\left[A_0^2\right] = 0$, then the attenuation anisotropy is

$$\frac{Q_x^{-1}(r)}{Q_z^{-1}(r)} = \frac{\ln\left[A^2(r)\big|_x\right]}{\ln\left[A^2(r)\big|_z\right]}. \tag{11}$$

Here, the wavefield is also rescaled with the same weight as the background wavefield.

Note the practicality of definitions in this paper for both the attenuation and its anisotropy. Seismic waves propagate away spherically from a single point source and the horizontal and vertical components *u* and *v* are used to measure the attenuations Q_x^{-1} and Q_z^{-1}, respectively. If both Q_x^{-1} and Q_z^{-1} can be evaluated from the horizontal and vertical components of field seismic data, the ratio of Q_x^{-1} and Q_z^{-1} can pragmatically reflect the directional variation of the attenuation. The property variation versus the direction is generally referred to as the anisotropy.

Theoretically, the horizontal attenuation (say Q_{11}^{-1}) ought to be measured from a plane-wave propagating parallel to the fracture direction and the vertical attenuation (Q_{33}^{-1}) should be measured from a plane-wave propagating perpendicularly to the fracture direction (Carcione 2000). Then, the anisotropy should be defined by the ratio of Q_{11}^{-1} and Q_{33}^{-1} (Zhu and Tsvankin 2007). However, how to measure these theoretical quantities from field seismic data which are generated from point sources is an unsolved issue. The relationship between (Q_x^{-1}, Q_z^{-1}) and (Q_{11}^{-1}, Q_{33}^{-1}) is not established either.

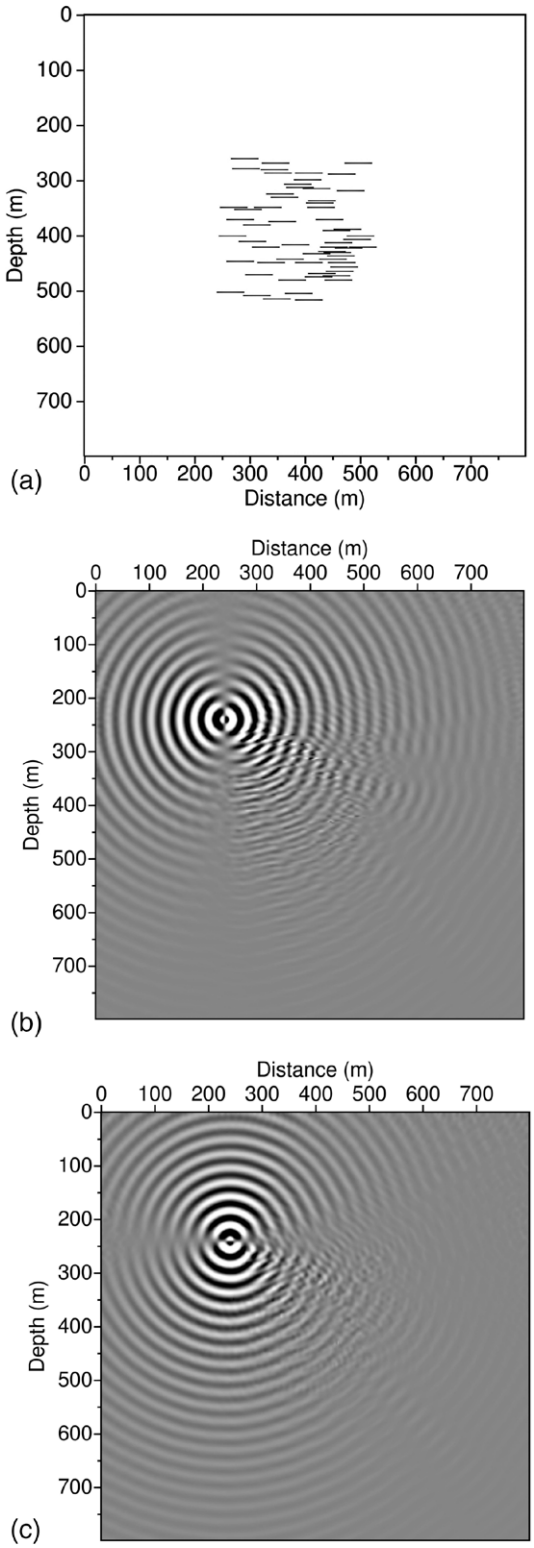


Figure 2. (*a*) A fractured model with random fracture distribution. (*b*) The horizontal component of the plane wave field. (*c*) The vertical components. The mono-frequency is 150 Hz.

Downloaded from https://academic.oup.com/jge/article/12/1/26/5110308 by Imperial College London Library user on 17 August 2020

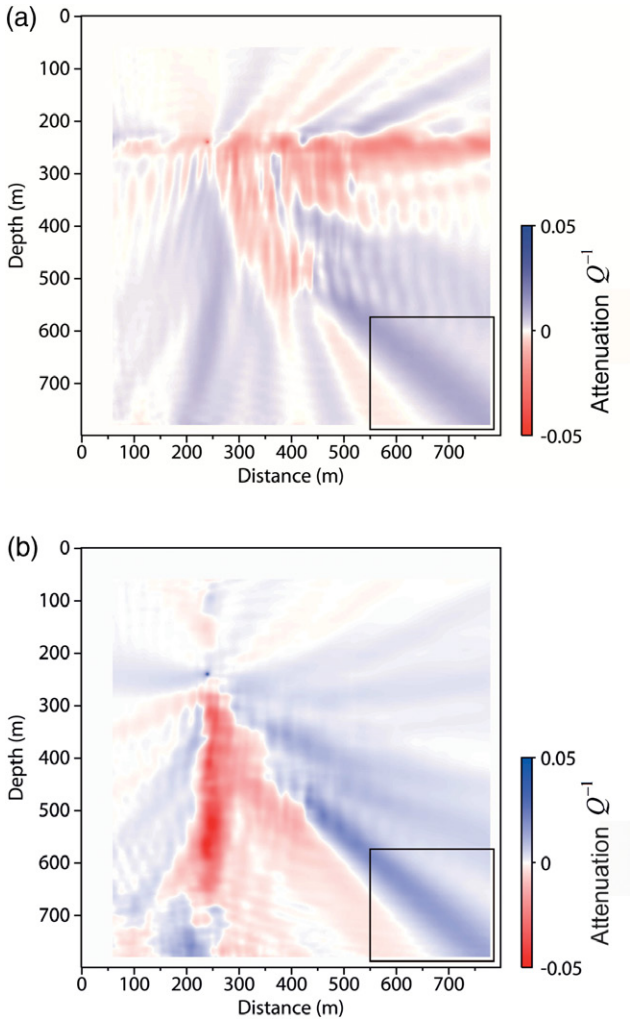


Figure 3. (*a*) The horizontal attenuation Q_x^{-1}. (*b*) The vertical attenuation Q_z^{-1}. They are evaluated from the horizontal and vertical components (figures 2(*b*) and (*c*), respectively) of the plane wavefield.

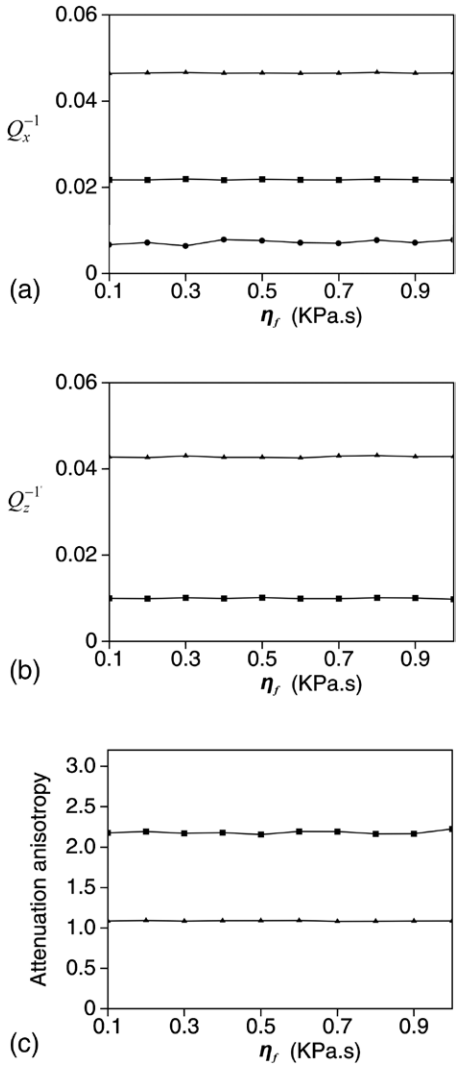


Figure 4. The effect of viscosity inside fractures: (*a*) the horizontal attenuation Q_x^{-1}, (*b*) the vertical attenuation Q_z^{-1}, and (*c*) the attenuation anisotropy γ. In the model, the porosity inside of fractures is 50% and $\lambda_f + 2\mu_f = 10^5$ KPa. The frequencies are 50 Hz (circles), 100 Hz (squares) and 150 Hz (triangles), respectively. For frequency 50 Hz, Q_z^{-1} is almost zero and γ would be infinite. These two curves could not plotted inside the frame.

Figure 3 shows the horizontal attenuation Q_x^{-1} and the vertical attenuation Q_z^{-1} extracted from components in figures 2(*b*) and (*c*), respectively. The negative value (in red) along the horizontal direction in figure 3(*a*) might be the interference caused by post-critical reflections (with the incident angles towards nearly 90°) and the negative value along the vertical direction in figure 3(*b*) might be the interference of multiples between fractures. To avoid these interferences for the attenuation evaluation, the energy in a 240 × 240 m^2 window at the bottom-right corner is selected to calculate the average attenuation.

Three parameters, i.e. viscosity, porosity and Lamé parameters of infill materials including fluid, will be tested to find out the key dynamic parameters of fractures that affect seismic attenuation.

4. The effect of viscosity

Viscosity is a fluid property indicating the resistance of the fluid to deformation due to a shear force. It can also be considered to be a measurement of fluid resistance to flow. Thick oil generally has a viscosity > 0.050 Pa·s and for reference, viscosity of bitumen can have a much higher viscosity of up to 1 KPa·s.

Figure 4 shows the horizontal attenuation Q_x^{-1}, the vertical attenuation Q_z^{-1}, and the attenuation anisotropy γ extracted from a synthetic wavefield. The porosity ϕ inside fractures is set to be 50% and $\lambda_f + 2\mu_f = 10^5$ KPa. Both figures 4(*a*) and (*b*) indicate that neither Q_x^{-1} nor Q_z^{-1} shows any dependency on the variation in viscosity η_f. As discussed in equation (6), because of the difference in order of magnitude between the viscosity and the Lamé parameters, the viscosity has no effect on $|C_N|$ and $|C_T|$ and in turn on the elastic constants c_{ij}.

However, for low frequency (100 Hz), the magnitudes of Q_x^{-1} and Q_z^{-1} are different. They lead to a significant anisotropic effect in the attenuation. For frequency 50 Hz, the value Q_z^{-1} is almost zero (a very small negative value) and the anisotropic effect γ would be much more significant (towards

Downloaded from https://academic.oup.com/jge/article/12/1/26/5110308 by Imperial College London Library user on 17 August 2020

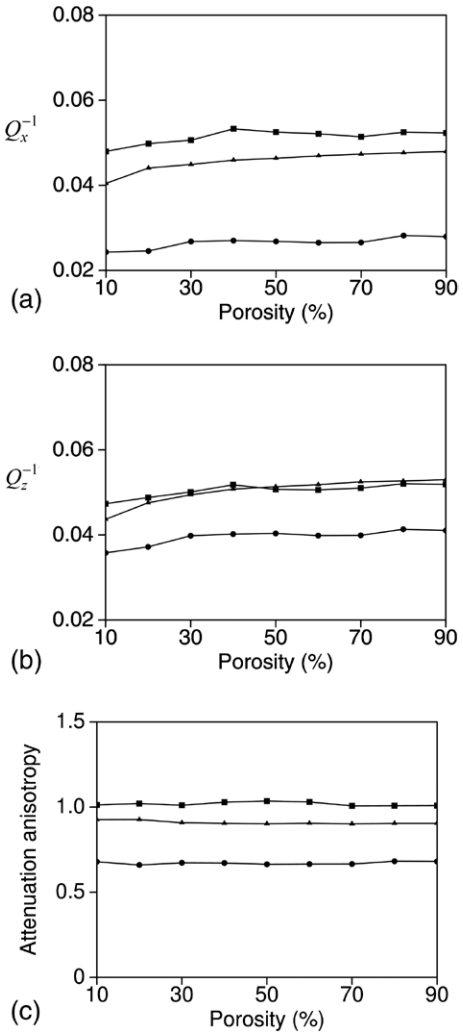


Figure 5. The effect of porosity within fractures: (*a*) the horizontal attenuation Q_x^{-1}, (*b*) the vertical attenuation Q_z^{-1}, and (*c*) the attenuation anisotropy γ. Measurements are extracted from plane wavefields with frequencies of 50 Hz (circles), 100 Hz (squares) and 150 Hz (triangles), respectively. In the model, viscosity η_f of infill fluid is 0.3 kPa.s.

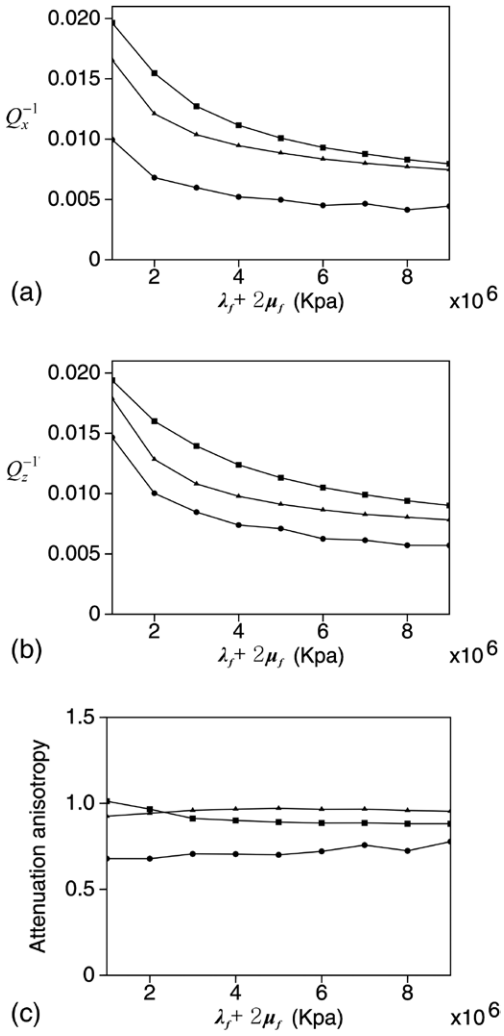


Figure 6. The effect of Lamé parameters on (*a*) the horizontal attenuation Q_x^{-1}, (*b*) the vertical attenuation Q_z^{-1}, and (*c*) the attenuation anisotropy γ. The values are extracted from plane wavefield with frequencies of 50 Hz (circles), 100 Hz (squares) and 150 Hz (triangles).

infinite). These two curves (Q_z^{-1} and γ for frequency 50 Hz) could not be plotted inside the frame and are therefore not shown in the figure.

5. The effect of porosity

Figures 5(*a*) and (*b*) show the relationship between porosity, Q_x^{-1} and Q_z^{-1}, and the attenuation for different plane waves with frequencies of 50, 100 and 150 Hz. Both attenuation Q_x^{-1} and Q_z^{-1} increase as porosity increases. When $\phi < 30\%$, the attenuation Q_z^{-1} increases fast, whereas when $\phi > 30\%$, it increases slowly. According to equation(3), porosity ϕ acts through the following inverse factor,

$$\left(1 + \frac{\lambda + 2\mu}{\mu}\phi C_N\right)^{-1} = \left(1 + \frac{\lambda + 2\mu}{\lambda_f + 2\mu_f + i\frac{4}{3}\omega\eta_f}\phi\right)^{-1}. \quad (12)$$

In this example, $\lambda = 2 \times 10^7$ Kpa, $\mu = 10^7$ Kpa and $\left(\lambda_f + 2\mu_f\right) = 10^6$ Kpa. The porosity is varied from 10 to 90% inside the fractures.

$$\left(1 + \frac{\lambda + 2\mu}{\lambda_f + 2\mu_f + i\frac{4}{3}\omega\eta_f}\phi\right)^{-1} \rightarrow \frac{1}{1 + 40\phi}. \quad (13)$$

This expression might offer us some insight into the inverse property of the porosity effect.

Figure 5(*c*) illustrates that the attenuation anisotropy γ has no dependency on porosity ϕ. However, it indicates clearly that the porosity has a significant effect on the attenuation anisotropy when the frequency is 50 Hz, but has less effect on the attenuation anisotropy when the frequency is either 100 or 150 Hz.

6. The effect of Lamé parameters

Figures 6(*a*) and (*b*) show that the Lamé parameters $\lambda_f + 2\mu_f$ have a direct effect on the attenuation. For all three sample

Downloaded from https://academic.oup.com/jge/article/12/1/26/5110308 by Imperial College London Library user on 17 August 2020

frequencies, 50, 100 or 150 Hz, both the horizontal attenuation Q_x^{-1} and the vertical attenuation Q_z^{-1} decrease when $\lambda_f + 2\mu_f$ within the fracture increases.

Figure 6(*c*) illustrates that the attenuation anisotropy γ has a negligible dependency on the variation of the Lamé parameters $\left(\lambda_f + 2\mu_f\right)$, and that it has higher anisotropy effect for frequency 50 Hz than others with 100 and 150 Hz.

In this example, the porosity ϕ is fixed to 10% and other parameters are set the same as those used in figure 5. The Lamé parameter $\left(\lambda_f + 2\mu_f\right)$ varies from 1 to 9 $\times$ 10^6 KPa.

In summary, for any single frequency, the attenuation anisotropy has a limited sensitivity to the value variation of any parameter, while for different frequencies, low-frequency results show stronger anisotropy attenuation for all three parameters.

7. Conclusions

Wave propagation through fractured media is simulated using a frequency-domain wave equation method. The media are treated as the effective anisotropic media and fractures are represented by frequency-dependent elastic constants. The effects of fractured materials are measured numerically based on the attenuation and the attenuation anisotropy.

Regarding the attenuation, the investigation reveals the following conclusions:

(1) The variation in viscosity η_f within fractures has no obvious effect on the attenuation. When porosity ϕ increases, the attenuation is increased. When Lamé parameters $\left(\lambda_f + 2\mu_f\right)$ increase, the attenuation is decreased.
(2) Seismic attenuation is more sensitive to the Lamé parameters $\left(\lambda_f + 2\mu_f\right)$ than to porosity and has a very limited sensitivity to the viscosity.

Regarding the attenuation anisotropy, the numerical evaluation suggests that:

(3) The variation in the attenuation anisotropy has no direct dependency on the variation of all three types of parameters, but the magnitude of the attenuation anisotropy depends on the frequency.
(4) Low frequencies have more anisotropic effect than high frequencies and 50 Hz has the strongest anisotropy effect if compared to 100 and 150 Hz.
(5) The attenuation anisotropy for a low frequency (say 50 Hz) is more sensitive to the viscosity than to the porosity and the Lamé parameters have the weakest effect on the anisotropy among these three parameters.

This numerical investigation suggests that low-frequency attenuation and especially the attenuation anisotropy are key measurements for detecting fluid within fractured media.

Acknowledgments

The authors are grateful to the National Natural Science Foundation of China (grant nos. 41104082, U1262207, 41474111) and the sponsors of the Centre for Reservoir Geophysics, Imperial College London, for supporting this research.

References

Biot M A 1962 Mechanics of deformation and acoustic propagation in porous media *J. Appl. Phys.* **33** 1482–98
Brajanovski M, Gurevich B and Schoenberg M 2005 A model for P-wave attenuation and dispersion in a porous medium permeated by aligned fractures *Geophys. J. Int.* **163** 372–84
Carcione J M 2000 A model for seismic velocity and attenuation in petroleum source rocks *Geophysics* **65** 1080–92
Coates R T and Schoenberg M 1995 Finite-difference modelling of faults and fractures *Geophysics* **60** 1514–26
Chapman M 2003 Frequency dependent anisotropy due to meso-scale fractures in the presence of equant porosity *Geophys. Prospect.* **51** 369–79
Hall F and Wang Y 2009 Elastic wave modelling by an integrated finite difference method *Geophys. J. Int.* **177** 104–14
Hall F and Wang Y 2012 Seismic response of fractures by numerical simulation *Geophys. J. Int.* **189** 591–601
Hudson J A, Liu E and Crampin S 1996 The mechanical properties of materials with interconnected cracks and pores *Geophys. J. Int.* **124** 105–12
Hudson J A, Pointer T and Liu E 2001 Effective-medium theories for fluid-saturated materials with aligned cracks *Geophys. Prospect.* **49** 509–22
Liu E, Hudson J A and Pointer T 2000 Equivalent medium representation of fractured rock *J. Geophys. Res.* **105** 2981–3000
Liu E and Martinez A 2013 *Seismic Fracture Characterization: Concepts and Practical Applications* (Houten: EAGE)
Maultzsch S, Chapman M, Liu E and Li X 2003 Modelling frequencydependent seismic anisotropy in fluid-saturated rock with aligned fractures: implication of fracture size estimation from anisotropic measurements *Geophys. Prospect.* **51** 381–92
Rao Y and Wang Y 2009 Fracture effects in seismic attenuation images reconstructed by waveform tomography *Geophysics* **74** R25–34
Schoenberg M 1980 Elastic wave behaviour across linear slip interfaces *J. Acoust. Soc. Am.* **68** 1516–21
Shen F and Toksöz M N 2000 Scattering characteristics in heterogeneously fractured reservoirs from waveform estimation *Geophys. J. Int.* **140** 251–66
Štekl I and Pratt R G 1998 Accurate viscoelastic modelling by frequency-domain finite differences using rotated operators *Geophysics* **63** 1779–94
Thomsen L 1995 Elastic anisotropy due to aligned cracks in porous rock *Geophys. Prospect.* **43** 805–29
Tod S R 2001 The effects on seismic waves of interconnected nearly aligned cracks *Geophys. J. Int.* **146** 249–63
Vlastos S, Liu E, Main I G and Narteau C 2007 Numerical simulation of wave propagation in 2D fractured media: scattering attenuation at different stages of the growth of a fracture population *Geophys. J. Int.* **171** 865–80
Wang Y 2004 Q analysis on reflection seismic data *Geophys. Res. Lett.* **31** L17606
Wang Y 2008 *Seismic Inverse Q Filtering* (Oxford: Blackwell)
Wang Y 2011 Seismic waveform modelling and tomography *Encyclopedia of Solid Earth Geophysics* ed H Gupta (Dordrecht: Springer) pp 1290–301
Wang Y and Rao Y 2009 Reflection seismic waveform tomography *J. Geophys. Res.* **114** B03304
Zhu Y and Tsvankin I 2007 Plane-wave attenuation anisotropy in orthorhombic media *Geophysics* **72** D9–19

Downloaded from https://academic.oup.com/jge/article/12/1/26/5110308 by Imperial College London Library user on 17 August 2020